International Journal of Bifurcation and Chaos, Vol. 22, No. 9 (2012) 1250218 (20 pages)

DOI: 10.1142/S0218127412502185

PROBING THE LOCAL DYNAMICS OF PERIODIC ORBITS BY THE GENERALIZED ALIGNMENT INDEX (GALI) METHOD

T. MANOS
University of Nova Gorica, School of Applied Sciences,
Vipavska 11c, SI-5270, Ajdovščina, Slovenia
Center for Research and Applications of Nonlinear Systems,
University of Patras, GR-26500, Patras, Greece
thanosm@master.math.upatras.gr

CH. SKOKOS
Max Planck Institute for the Physics of Complex Systems,
Nöthnitzer Str. 38, D-01187, Dresden, Germany
Center for Research and Applications of Nonlinear Systems,
University of Patras, GR-26500, Patras, Greece
hskokos@pks.mpg.de

CH. ANTONOPOULOS
Interdisciplinary Center for Nonlinear Phenomena
and Complex Systems (CENOLI),
Service de Physique des Systèmes Complexes et Mécanique Statistique,
Université Libre de Bruxelles, 1050, Brussels, Belgium
cantonop@ulb.ac.be

Received March 3, 2011; Revised July 12, 2011

As originally formulated, the Generalized Alignment Index (GALI) method of chaos detection has so far been applied to distinguish quasiperiodic from chaotic motion in conservative nonlinear dynamical systems. In this paper, we extend its realm of applicability by using it to investigate the local dynamics of *periodic* orbits. We show theoretically and verify numerically that for *stable* periodic orbits, the GALIs tend to zero following particular power laws for Hamiltonian flows, while they fluctuate around nonzero values for symplectic maps. By comparison, the GALIs of *unstable* periodic orbits tend exponentially to zero, both for flows and maps. We also apply the GALIs for investigating the dynamics in the neighborhood of periodic orbits, and show that for chaotic solutions influenced by the homoclinic tangle of unstable periodic orbits, the GALIs can exhibit a remarkable oscillatory behavior during which their amplitudes change by many orders of magnitude. Finally, we use the GALI method to elucidate further the connection between the dynamics of Hamiltonian flows and symplectic maps. In particular, we show that, using the components of deviation vectors orthogonal to the direction of motion for the computation of GALIs, the indices of stable periodic orbits behave for flows as they do for maps.

Keywords: GALI method; periodic orbits; Hamiltonian flows; symplectic maps.

1. Introduction

The method of the Generalized Alignment Indices (GALIs) was originally introduced in [Skokos *et al.*, 2007] as an efficient chaos detection method. To date, the GALI method has been successfully applied to a wide variety of conservative dynamical systems for the discrimination between regular and chaotic motion, as well as for the detection of regular motion on low dimensional tori [Antonopoulos & Bountis, 2006; Christodoulidi & Bountis, 2006; Skokos *et al.*, 2008; Manos *et al.*, 2008a, 2009; Bountis *et al.*, 2009; Skokos & Gerlach, 2010; Manos & Ruffo, 2011; Manos & Athanassoula, 2011; Gerlach *et al.*, 2012].

In the present paper, we extend and complete the study of the GALI method, focusing on its behavior for the special case of periodic orbits and their neighborhood in conservative dynamical systems. The detection of periodic orbits and the determination of their stability are fundamental approaches for the study of nonlinear dynamical systems, since they provide valuable information for the structure of their phase space. In particular, stable periodic orbits are associated with regular motion, since they are surrounded by tori of quasiperiodic motion, while in the vicinity of unstable periodic orbits chaotic motion occurs.

The GALI method is related to the evolution of several deviation vectors from the studied orbit, and therefore is influenced by the characteristics of the system's tangent space. The main goal of the paper is to determine the usefulness of the method for probing the local dynamics of periodic orbits with different stability types. We manage to achieve this goal by deriving theoretical predictions for the behavior of GALIs for stable and unstable periodic orbits. We also verify numerically the validity of these predictions, by studying the evolution of GALIs for periodic orbits of several Hamiltonian flows and symplectic maps, clarifying also the connections of such dynamical systems. In addition, we show how the properties of the index can be used to locate stable periodic orbits, and to understand the dynamics in the vicinity of unstable ones.

The paper is organized as follows: in the first two introductory sections, we recall the definition of the GALI, describing also its behavior for regular and chaotic orbits (Sec. 2), and report the several stability types of periodic orbits in conservative systems (Sec. 3). In Sec. 4, we first study theoretically the behavior of the index for stable and unstable orbits, and then present applications of the GALI to particular orbits of Hamiltonian flows and symplectic maps. Section 5 is devoted to the dynamics in the neighborhood of periodic orbits, while Sec. 6 is dedicated to the relation between the GALIs of stable periodic orbits for flows and maps. Finally, in Sec. 7, we summarize our results.

2. The Generalized Alignment Index (GALI)

Let us briefly recall the definition of the GALIs and their behavior for regular and chaotic motion in conservative dynamical systems. Consider an autonomous Hamiltonian system of N degrees of freedom (Ndof), described by the Hamiltonian $H(q_1, q_2, \ldots, q_N, p_1, p_2, \ldots, p_N)$, where q_i and p_i, $i = 1, 2, \ldots, N$ are the generalized coordinates and conjugate momenta, respectively. An orbit in the $2N$-dimensional phase space $\mathcal{S}$ of this system is defined by a vector $\mathbf{x}(t) = (q_1(t), q_2(t), \ldots, q_N(t), p_1(t), p_2(t), \ldots, p_N(t))$, with $x_i = q_i$, $x_{i+N} = p_i$, $i = 1, 2, \ldots, N$. The time evolution of this orbit is governed by Hamilton's equations of motion

$$\frac{d\mathbf{x}}{dt} = \boldsymbol{\mathcal{V}}(\mathbf{x}) = \left(\frac{\partial H}{\partial \mathbf{p}}, -\frac{\partial H}{\partial \mathbf{q}}\right), \tag{1}$$

while the time evolution of an initial deviation vector $\mathbf{w}(0) = (dx_1(0), \ldots, dx_{2N}(0))$ from the $\mathbf{x}(t)$ solution of Eq. (1), obeys the variational equations

$$\frac{d\mathbf{w}}{dt} = \mathbf{M}(\mathbf{x}(t)) \cdot \mathbf{w}, \tag{2}$$

where $\mathbf{M} = \partial \boldsymbol{\mathcal{V}} / \partial \mathbf{x}$ is the Jacobian matrix of $\boldsymbol{\mathcal{V}}$.

Let us also consider a discrete time $t = n \in \mathbb{N}$ conservative dynamical system defined by a $2N$-dimensional ($2N$D) symplectic map F. The evolution of an orbit in the $2N$-dimensional space $\mathcal{S}$ of the map is governed by the difference equation

$$\mathbf{x}(n+1) \equiv \mathbf{x}_{n+1} = F(\mathbf{x}_n). \tag{3}$$

In this case, the evolution of a deviation vector $\mathbf{w}(n) \equiv \mathbf{w}_n$, with respect to a reference orbit $\mathbf{x}_n$, is given by the corresponding *tangent map*

$$\mathbf{w}(n+1) \equiv \mathbf{w}_{n+1} = \frac{\partial F}{\partial \mathbf{x}}(\mathbf{x}_n) \cdot \mathbf{w}_n. \tag{4}$$

For Ndof Hamiltonian flows and $2N$D maps the Generalized Alignment Index of order k (GALI$_k$), $2 \leq k \leq 2N$, is determined through the evolution of k initially linearly independent deviation vectors $\mathbf{w}_k(0)$. To avoid overflow problems, the resulting deviation vectors $\mathbf{w}_k(t)$ are continually normalized, but their directions are kept intact. Then, according to [Skokos *et al.*, 2007] GALI$_k$ is defined as the volume of the k-parallelogram having as edges k unit deviation vectors $\hat{w}_i(t) = \mathbf{w}_i(t)/\|\mathbf{w}_i(t)\|$, $i = 1, 2, \ldots, k$, determined through the wedge product of these vectors as

$$\text{GALI}_k(t) = \|\hat{w}_1(t) \wedge \hat{w}_2(t) \wedge \cdots \wedge \hat{w}_k(t)\|, \quad (5)$$

with $\|\cdot\|$ denoting the usual norm. From this definition it is evident that if at least two of the deviation vectors become linearly dependent, the wedge product in Eq. (5) becomes zero and the GALI$_k$ vanishes.

In the $2N$-dimensional phase space $\mathcal{S}$ of an Ndof Hamiltonian flow or a $2N$D map, regular orbits lie on s-dimensional tori, with $2 \leq s \leq N$ for Hamiltonian flows, and $1 \leq s \leq N$ for maps. For such orbits, all deviation vectors tend to fall on the s-dimensional tangent space of the torus on which the motion lies. Thus, if we start with $k \leq s$ general deviation vectors, these will remain linearly independent on the s-dimensional tangent space of the torus, since there is no particular reason for them to become linearly dependent. As a consequence GALI$_k$ remains practically constant and different from zero for $k \leq s$. On the other hand, GALI$_k$ tends to zero for $k > s$, since some deviation vectors will eventually have to become linearly dependent. In particular, the generic behavior of GALI$_k$ for regular orbits lying on s-dimensional tori is given by [Christodoulidi & Bountis, 2006; Skokos *et al.*, 2008]

$$\text{GALI}_k(t) \propto \begin{cases} \text{constant} & \text{if } 2 \leq k \leq s \\ \dfrac{1}{t^{k-s}} & \text{if } s < k \leq 2N - s \\ \dfrac{1}{t^{2(k-N)}} & \text{if } 2N - s < k \leq 2N. \end{cases} \quad (6)$$

Note that these estimations are valid only when the conditions stated above are exactly satisfied. For example, in the case of 2D maps, where the only possible torus is a one-dimensional ($s = 1$) invariant curve, the tangent space is one-dimensional. Thus, the behavior of GALI$_2$ (which is the only possible index in this case) is given by the third branch of Eq. (6), i.e. GALI$_2 \propto 1/t^2$, since the first two cases of Eq. (6) are not applicable. From Eq. (6) we deduce that, for the usual case of regular orbits lying on an N-dimensional torus, the behavior of GALI$_k$ is given by

$$\text{GALI}_k(t) \propto \begin{cases} \text{constant} & \text{if } 2 \leq k \leq N \\ \dfrac{1}{t^{2(k-N)}} & \text{if } N < k \leq 2N. \end{cases} \quad (7)$$

On the other hand, for a chaotic orbit all deviation vectors tend to become linearly *dependent*, aligning themselves in the direction defined by the maximum Lyapunov characteristic exponent (mLCE) and hence, in that case, GALI$_k$ tends to zero *exponentially* following the law [Skokos *et al.*, 2007]

$$\text{GALI}_k(t) \propto e^{-[(\sigma_1-\sigma_2)+(\sigma_1-\sigma_3)+\cdots+(\sigma_1-\sigma_k)]t}, \quad (8)$$

where $\sigma_1, \ldots, \sigma_k$ are the first k largest Lyapunov characteristic exponents (LCEs) of the orbit.

The GALI is a generalization of a similar indicator called the Smaller Alignment Index (SALI) [Skokos, 2001b; Skokos *et al.*, 2003, 2004], which has been used successfully for the detection of chaos in several dynamical systems [Széll *et al.*, 2004; Panagopoulos *et al.*, 2004; Bountis & Skokos, 2006; Capuzzo-Dolcetta *et al.*, 2007; Manos *et al.*, 2008b; Macek *et al.*, 2007; Stránský *et al.*, 2009; Macek *et al.*, 2010]. The generalization consists of the fact that the GALIs use information of *more than two* deviation vectors from the reference orbit, leading to a faster and clearer distinction between regular and chaotic motion compared with SALI. In practice, SALI is equivalent to GALI$_2$ since GALI$_2 \propto$ SALI (see Appendix B of [Skokos *et al.*, 2007] for more details).

For the numerical computation of GALIs we consider the $k \times 2N$ matrix $\mathbf{W}(t)$ having as rows the coordinates $w_{ij}(t)$ of the unit deviation vectors $\hat{w}_i(t)$, $i = 1, 2, \ldots, k$, $j = 1, 2, \ldots, 2N$, with respect to the usual orthonormal basis $\hat{e}_1 = (1, 0, 0, \ldots, 0)$, $\hat{e}_2 = (0, 1, 0, \ldots, 0), \ldots, \hat{e}_{2N} = (0, 0, 0, \ldots, 1)$ of the $2N$-dimensional tangent space $\mathcal{S}$. Thus, GALI$_k(t)$ can be evaluated as the square root of the sum of the squares of the determinants of all possible $k \times k$ submatrices of $\mathbf{W}$ [Skokos *et al.*, 2007]

$$\mathrm{GALI}_k = \left\{ \sum_{1\le i_1<i_2<\cdots<i_k\le 2N} \begin{vmatrix} w_{1i_1} & w_{1i_2} & \cdots & w_{1i_k} \\ w_{2i_1} & w_{2i_2} & \cdots & w_{2i_k} \\ \vdots & \vdots & & \vdots \\ w_{ki_1} & w_{ki_2} & \cdots & w_{ki_k} \end{vmatrix}^2 \right\}^{1/2} . \quad (9)$$

Here the sum is performed over all possible combinations of k indices out of $2N$, $|\cdot|$ denotes the determinant, and the explicit dependence of all quantities on time t is omitted for simplicity.

Equation (9) is ideal for the theoretical determination of the asymptotic behavior of GALIs for chaotic and regular orbits. It has been used in [Christodoulidi & Bountis, 2006; Skokos *et al.*, 2007, 2008] for the derivation of Eqs. (6) and (8), and will be applied later on in Sec. 4.1 for the determination of GALIs' behavior for periodic orbits. However, from a practical point of view the application of Eq. (9) for the numerical evaluation of GALI_k is not very efficient as it might require the computation of a large number of determinants. In [Antonopoulos & Bountis, 2006; Skokos *et al.*, 2008], a more efficient numerical technique for the computation of GALI_k, which is based on the Singular Value Decomposition of matrix $\mathbf{W}(t)$ was presented. In particular, it has been shown that GALI_k is equal to the product of the singular values $z_i \geq 0$, $i = 1, 2, \ldots, k$ of $\mathbf{W}^{\mathrm{T}}(t)$

$$\mathrm{GALI}_k(t) = \prod_{i=1}^{k} z_i(t), \quad (10)$$

where $(^{\mathrm{T}})$ denotes the transpose matrix.

3. Stability of Periodic Orbits

Now, consider a T-periodic orbit (i.e. an orbit satisfying $\mathbf{x}(t+T) = \mathbf{x}(t)$) of an Ndof Hamiltonian flow or of a $2N$D symplectic map. Its linear stability is determined by the eigenvalues of the so-called monodromy matrix $\mathbf{Y}(T)$, which is obtained from the solution of the variational equations for one period T (see for example [Broucke, 1969; Lichtenberg & Lieberman, 1992, Sec. 3.3; Skokos, 2001a; Hadjidemetriou, 2006; Cvitanović *et al.*, 2009, Chap. 4, 5]). The monodromy matrix is symplectic,[1] and its columns correspond to linearly independent solutions of the equations that govern the evolution of deviation vectors. In particular, the evolution of an initial deviation $\mathbf{w}(0)$ from a T-periodic orbit is given by

$$\mathbf{w}(iT) = [\mathbf{Y}(T)]^i \cdot \mathbf{w}(0), \quad i = 1, 2, \ldots . \quad (11)$$

Due to the symplectic nature of the monodromy matrix and the fact that its elements are real, the eigenvalues of $\mathbf{Y}(T)$ have the following property: if λ is an eigenvalue then $1/\lambda$ and the complex conjugate λ^* are also eigenvalues. This property shows that the eigenvalues $\lambda = 1$ and $\lambda = -1$ come in pairs and that complex eigenvalues with modulus not equal to 1 always appear in quartets. When all eigenvalues are on the unit circle, the corresponding periodic orbit is said to be *stable*. If there exist eigenvalues off the unit circle, the periodic orbit is *unstable*.

A few remarks on the connection of Hamiltonian systems with symplectic maps are necessary at this point. Since autonomous Hamiltonian systems are conservative, the constancy of the Hamiltonian function introduces a constraint which fixes an eigenvalue of the monodromy matrix to be equal to 1 and so, by the symplectic property, there must be a second eigenvalue equal to 1. Thus, for an Ndof Hamiltonian system there are only $2(N-1)$ *a priori* unknown eigenvalues, and so we can reduce our study to a $2(N-1)$-dimensional subspace of phase space $\mathcal{S}$. This subspace is obtained by the well-known method of the Poincaré surface of section (PSS) (e.g. [Lichtenberg & Lieberman, 1992, pp. 17–20; Cvitanović *et al.*, 2009, Sec. 3.1, 3.2]). The corresponding monodromy matrix of the periodic orbit is also symplectic. Thus, in this sense, an Ndof Hamiltonian system is dynamically equivalent to $2(N-1)$D symplectic map.

The different stability types of a periodic orbit in Hamiltonian systems of 2dof and 3dof (or equivalently in 2D and 4D maps) have been studied in detail in [Broucke, 1969; Hadjidemetriou, 1975; Dullin & Meiss, 1998; Hadjidemetriou, 2006], while the stability of periodic orbits in higher dimensional

[1] $\mathbf{Y}(T)$ satisfies the condition $\mathbf{Y}(T)^{\mathrm{T}} \cdot \mathbf{J}_{2N} \cdot \mathbf{Y}(T) = \mathbf{J}_{2N}$, with $\mathbf{J}_{2N} = \begin{bmatrix} \mathbf{0}_N & \mathbf{I}_N \\ -\mathbf{I}_N & \mathbf{0}_N \end{bmatrix}$, where $\mathbf{I}_N$ is the $N \times N$ identity matrix and $\mathbf{0}_N$ is the $N \times N$ zero matrix.

conservative systems was considered in [Howard & MacKay, 1987; Howard & Dullin, 1998; Skokos, 2001a]. Following the terminology introduced in [Skokos, 2001a], the general stability type of a periodic orbit of an Ndof Hamiltonian system, or equivalently a $2(N-1)$D map, is denoted by

$$S_p U_m \Delta_l, \quad \text{with } p+m+2l = N-1, \tag{12}$$

which means that p couples of eigenvalues are on the unit circle, m couples are on the real axis and l quartets are on the complex plane but off the unit circle and the real axis. We conclude that a periodic orbit is stable only when its stability type is S_{N-1}. In all other cases, the orbit is unstable since there exist eigenvalues of the monodromy matrix off the unit circle. For example, in the case of a 3dof Hamiltonian system or a 4D map, a periodic orbit can be linearly stable (S_2) or have three different types of instability: S_1U_1, U_2, Δ_1 (often called simple unstable, double unstable and complex unstable, respectively, see e.g. [Contopoulos & Magnenat, 1985]).

4. The Behavior of the GALI for Periodic Orbits

4.1. *Theoretical treatment*

Let λ_i, $i = 1, 2, \ldots, 2N$ be the (possibly complex) eigenvalues of the monodromy matrix $\mathbf{Y}(T)$ of a T-periodic orbit, ordered as $|\lambda_1| \geq |\lambda_2| \geq \cdots \geq |\lambda_{2N}|$. Then, the corresponding LCEs σ_i, $i = 1, 2, \ldots, 2N$ are given by [Benettin & Galgani, 1979; Benettin *et al.*, 1979; Skokos *et al.*, 2007; Skokos, 2010]

$$\sigma_i = \frac{1}{T} \ln |\lambda_i|. \tag{13}$$

In the case of unstable periodic orbits, where at least $|\lambda_1| > 1$, we get $\sigma_1 > 0$, which implies that nearby orbits diverge exponentially from the periodic trajectory. Unstable periodic orbits of nonintegrable Hamiltonian systems and symplectic maps are located inside chaotic domains. All nonperiodic chaotic orbits in these domains have the same spectrum of LCEs, which in general, differs from the spectrum of LCEs of the unstable periodic orbits of these domains.

For determining the behavior of GALI_k for unstable periodic orbits, one can apply the analysis presented in [Skokos *et al.*, 2007] for chaotic orbits which also have $\sigma_1 > 0$. This approach leads to the conclusion that GALI_k of unstable periodic orbits tends to zero exponentially following the law (8)

$$\mathrm{GALI}_k(t) \propto e^{-[(\sigma_1-\sigma_2)+(\sigma_1-\sigma_3)+\cdots+(\sigma_1-\sigma_k)]t}. \tag{14}$$

However, the case of stable periodic orbits needs a more careful investigation. For this purpose, let us consider an Ndof Hamiltonian system expressed in action-angle variables J_i, θ_i, $i = 1, 2, \ldots, N$. The equations of motion of a periodic orbit of this system are

$$\begin{aligned} \dot{J}_i &= -\frac{\partial H}{\partial \theta_i} = 0, \\ \dot{\theta}_i &= \frac{\partial H}{\partial J_i} = \omega_i(J_1, J_2, \ldots, J_N), \end{aligned} \qquad 1 \leq i \leq N. \tag{15}$$

The frequencies ω_i satisfy a relation of the form

$$\frac{\omega_1}{k_1} = \frac{\omega_2}{k_2} = \cdots = \frac{\omega_N}{k_N} = \Omega(J_1, J_2, \ldots, J_N), \tag{16}$$

where k_i, $i = 1, 2, \ldots, N$, are integer numbers and $\Omega(J_1, J_2, \ldots, J_N) = 2\pi/T$ with T being the period of the orbit. Equations (15) can be easily integrated to give

$$\begin{aligned} J_i(t) &= J_{i0}, \\ \theta_i(t) &= \theta_{i0} + \Omega(J_{10}, J_{20}, \ldots, J_{N0}) k_i t, \end{aligned} \qquad 1 \leq i \leq N, \tag{17}$$

where J_{i0}, θ_{i0}, $i = 1, 2, \ldots, N$ are the initial conditions.

Let us now denote by ξ_i, η_i, $i = 1, 2, \ldots, N$, small deviations from J_i and θ_i, respectively. Inserting Eqs. (15) and (16) into the variational equations of the Hamiltonian system we get

$$\dot{\xi}_i = 0, \quad \dot{\eta}_i = k_i \sum_{j=1}^{N} \Omega_j \xi_j, \quad 1 \leq i \leq N, \tag{18}$$

where $\Omega_j = \partial\Omega/\partial J_j$ are computed for the initial constant values J_{j0}, $j = 1, 2, \ldots, N$. Using as basis of the $2N$-dimensional tangent space of the Hamiltonian flow the $2N$ unit vectors $\{\hat{v}_1, \hat{v}_2, \ldots, \hat{v}_{2N}\}$, such that the first N of them correspond to the N action variables and the remaining ones to the N conjugate angle variables, any initial deviation vector $\mathbf{w}_i(0) = (\xi_1^i(0), \xi_2^i(0), \ldots, \xi_N^i(0), \eta_1^i(0), \eta_2^i(0), \ldots, \eta_N^i(0))$, evolves in time as

$$\mathbf{w}_i(t) = \sum_{j=1}^{N} \xi_j^i(0)\hat{v}_j + \sum_{j=1}^{N} \left[\eta_j^i(0) + \left(\sum_{l=1}^{N} \Omega_l \xi_l^i(0) \right) k_j t \right] \hat{v}_{N+j}. \quad (19)$$

From the above, it readily follows that for sufficiently long times $\|\mathbf{w}_i(t)\| \propto t$.

Let us now consider k, initially linearly independent, randomly chosen, unit deviation vectors $\{\hat{w}_1, \ldots, \hat{w}_k\}$, with $2 \leq k \leq 2N$, and let $\mathbf{W}$ be the matrix having as rows the coordinates of these vectors with respect to the $\{\hat{v}_1, \hat{v}_2, \ldots, \hat{v}_{2N}\}$ basis. Defining by $\boldsymbol{\xi}_i^k$ and $\boldsymbol{\eta}_i^k$, $i = 1, 2, \ldots, N$, the $k \times 1$ column matrices

$$\boldsymbol{\xi}_i^k = [\xi_i^1(0) \quad \xi_i^2(0) \quad \ldots \quad \xi_i^k(0)]^{\mathrm{T}}, \quad \boldsymbol{\eta}_i^k = [\eta_i^1(0) \quad \eta_i^2(0) \quad \ldots \quad \eta_i^k(0)]^{\mathrm{T}}, \quad (20)$$

$\mathbf{W}(t)$ assumes the form

$$\mathbf{W}(t) \propto \frac{1}{t^k} \cdot \mathbf{W}^k(t) = \frac{1}{t^k} \left[\boldsymbol{\xi}_1^k \quad \ldots \quad \boldsymbol{\xi}_N^k \quad \left(\boldsymbol{\eta}_1^k + \left[\sum_{l=1}^{N} \Omega_l \boldsymbol{\xi}_l^k \right] k_1 t \right) \quad \ldots \quad \left(\boldsymbol{\eta}_N^k + \left[\sum_{l=1}^{N} \Omega_l \boldsymbol{\xi}_l^k \right] k_N t \right) \right], \quad (21)$$

where we have considered $\prod_{i=1}^{k} \|\mathbf{w}_i(t)\| \propto t^k$. Then, Eq. (9) can be used for the computation of GALI_k.

In order to determine the leading order behavior of GALI_k as t grows, we look for the fastest increasing determinants of all $k \times k$ minors of matrix $\mathbf{W}^k$. For $2 \leq k \leq 2N-1$, these determinants include only one column of $\mathbf{W}^k$ containing the term $[\sum_{l=1}^{N} \Omega_l \boldsymbol{\xi}_l^k]$ and grow proportional to t, since determinants with more than one column proportional to $[\sum_{l=1}^{N} \Omega_l \boldsymbol{\xi}_l^k]$ are identically zero. Thus, we conclude that $\mathrm{GALI}_k(t) \propto t^{-(k-1)}$ for $2 \leq k \leq 2N-1$. For $k = 2N$, $\mathbf{W}^k$ is a square $2N \times 2N$ matrix which has a constant determinant, since time appears only through multiplications with the N first columns of $\mathbf{W}^k$, and so $\mathrm{GALI}_k(t) \propto t^{-2N}$. Summarizing, the time evolution of GALI_k for stable periodic orbits of Ndof Hamiltonian systems is given by

$$\mathrm{GALI}_k \propto \begin{cases} \dfrac{1}{t^{k-1}} & \text{if } 2 \leq k \leq 2N-1 \\ \dfrac{1}{t^{2N}} & \text{if } k = 2N. \end{cases} \quad (22)$$

It is worth mentioning that Eq. (22) can be retrieved from Eq. (6) by assuming motion on a one-dimensional ($s = 1$) torus, i.e. on a one-dimensional curve, which is the stable periodic orbit. Note that for $s = 1$, only the last two branches of Eq. (6) are meaningful.

Stable periodic orbits of symplectic maps correspond to stable fixed points of the map, which are located inside islands of stability. Any deviation vector from the stable periodic orbit performs a rotation around the fixed point. This, for example, can be easily seen in the case of 2D maps where the islands in the vicinity of a stable fixed point can be represented through linearization, by ellipses (see for instance [Lichtenberg & Lieberman, 1992, Sec. 3.3.b; Lega & Froeschlé, 2001]). Thus, any set of $2 \leq k \leq 2N$ initially linearly independent, unit deviation vectors will rotate around the fixed point, keeping, on the average, the angles between them constant. This means that the volume of the k-parallelogram having as edges these vectors will remain practically constant, exhibiting some fluctuations, since the rotation angles are constant only on average. So, in the case of stable periodic orbits of $2N$D maps we have

$$\mathrm{GALI}_k \propto \text{const}, \quad 2 \leq k \leq 2N. \quad (23)$$

4.2. *Numerical results — Hamiltonian flows*

To verify the validity of the theoretical predictions of Eqs. (14) and (22) we now compute the GALIs for some representative Hamiltonian systems of different number of degrees of freedom.

4.2.1. *2dof Hénon–Heiles system*

First we consider the well-known 2dof Hénon–Heiles model [Hénon & Heiles, 1964]

$$H_2 = \frac{1}{2}(p_x^2 + p_y^2) + \frac{1}{2}(x^2 + y^2) + x^2 y - \frac{1}{3} y^3. \quad (24)$$

In our study we keep the value of the Hamiltonian fixed at $H_2 = 0.125$. Figure 1(a) shows the PSS of the system defined by $x = 0$, $p_x \geq 0$. We consider two stable periodic orbits (whose stability type is S_1 according to Eq. (12)): An orbit of period 5 (i.e. an orbit intersecting the PSS at the five points denoted by blue crosses in Fig. 1(a)) with initial condition $(x, y, p_x, p_y) \approx (0, 0.35207, 0.36427, 0.14979)$, and an orbit of period 7 (red squares in Fig. 1(a)) with initial condition $(x, y, p_x, p_y) \approx (0, 0.45882, 0.32229, 0)$. The time evolution of GALI_k, $k = 2, 3, 4$ for these two orbits, for a random choice of initial orthonormal deviation vectors, is shown in Figs. 1(b) and 1(c), respectively. For both orbits the indices show a power law decay to zero, in accordance with the theoretical prediction of Eq. (22) for $N = 2$.

In order to check the validity of Eq. (14), we consider an unstable periodic orbit (of U_1 type) of period 5 (green circles in Fig. 1(a)) with initial condition $(x, y, p_x, p_y) \approx (0, 0.2083772012, 0.4453146996, 0.1196065752)$. The theoretically expected value of this orbit's mLCE σ_1 is estimated from Eq. (13) to be $\sigma_1 \approx 0.084$, while $\sigma_2 = 0$ because the Hamiltonian function is an integral of motion.

In Fig. 1(d), the time evolution of the corresponding GALI_k, $k = 2, 3, 4$ is plotted. From these results we conclude that the computed values of GALIs are well approximated by Eq. (14) for $\sigma_1 = 0.084$ and $\sigma_2 = 0$, at least up to $t \approx 350$. After that time, we observe a change in the exponential decay of GALI_2. This happens because the numerically computed orbit deviates from the unstable periodic orbit, due to computational inaccuracies, and enters the surrounding chaotic domain, which is characterized by different LCEs. This behavior is also evident from the evolution of the finite time mLCE $L_1(t)$ [Fig. 1(e)] having as limit for $t \to \infty$ the mLCE σ_1 of the computed orbit (for more details on the computation of the mLCE, the reader is referred to [Skokos, 2010, Sec. 5]). For an initial time interval, $L_1(t)$ well approximates the mLCE of the unstable periodic orbit, but later on, due to the divergence of the computed orbit from the periodic trajectory, $L_1(t)$ tends to a different value, which is the mLCE of the chaotic domain around the unstable periodic orbit.

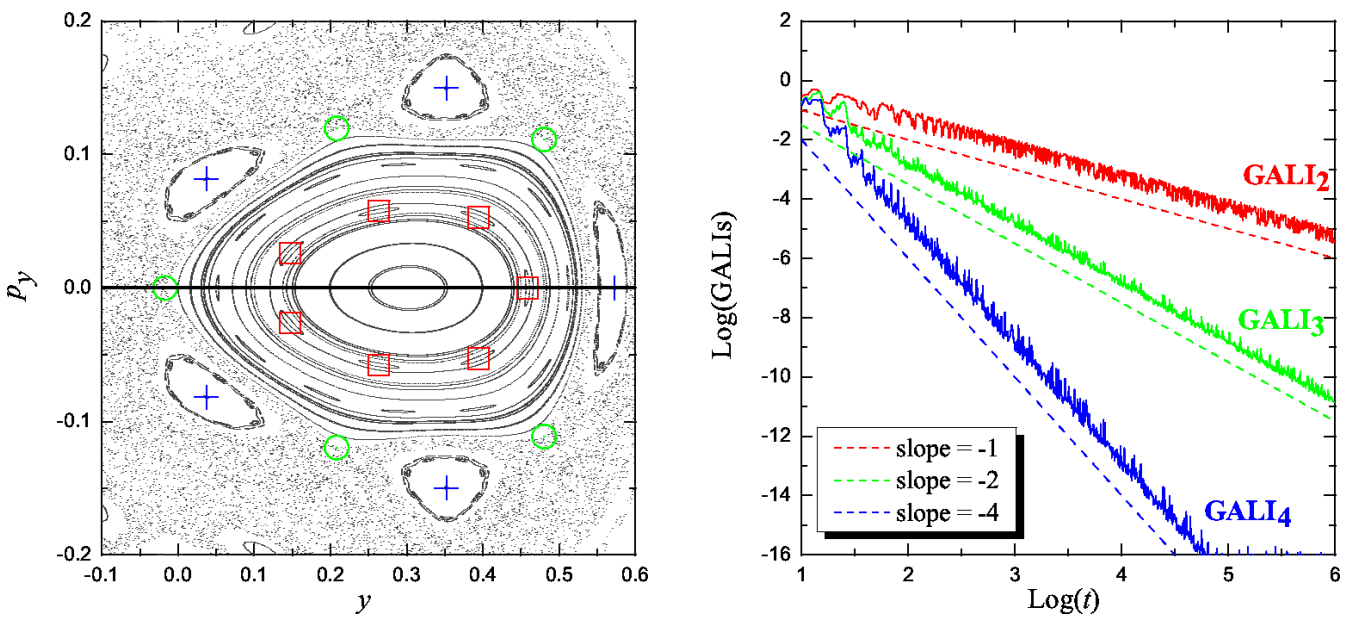

Fig. 1. (a) The PSS of the 2dof Hénon–Heiles system (24) with $H_2 = 0.125$. The intersection points of stable periodic orbits of periods 5 (blue crosses) and 7 (red squares), as well as an unstable orbit of period 5 (green circles) are also plotted. The line $p_y = 0$, denoting a set of initial conditions discussed in Sec. 5, is also plotted. The time evolution of GALI_2 (red curves), GALI_3 (green curves) and GALI_4 (blue curves) for these three orbits is shown in panels (b)–(d) respectively. Both axes of (b) and (c), and the vertical axis of (d) are logarithmic. (e) The time evolution of the quantity $L_1(t)$, which has as limit for $t \to \infty$ the mLCE σ_1 of the unstable periodic orbit (horizontal dotted line). Plotted lines correspond to functions proportional to t^{-1}, t^{-2} and t^{-4} in (b) and (c), and the exponential laws (14) for $\sigma_1 = 0.084$, $\sigma_2 = 0$ in (d).

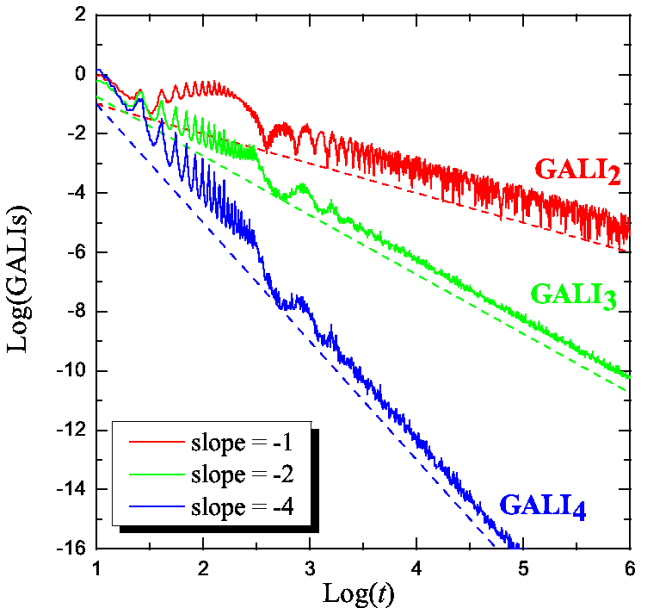

(c)

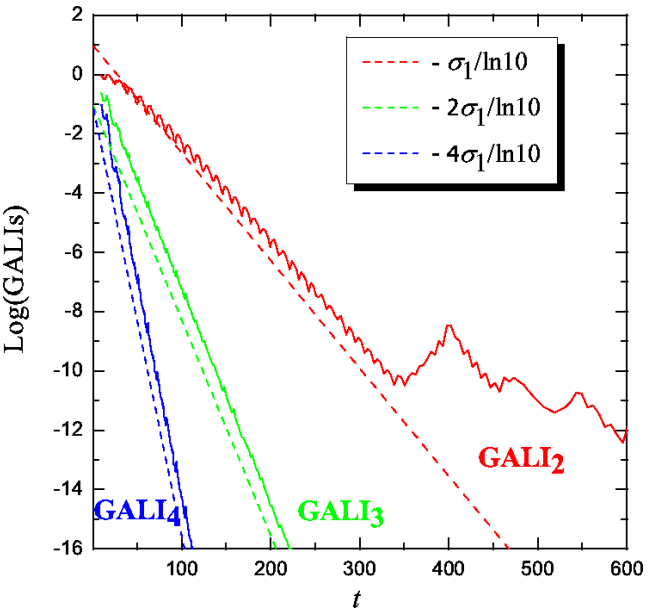

(d)

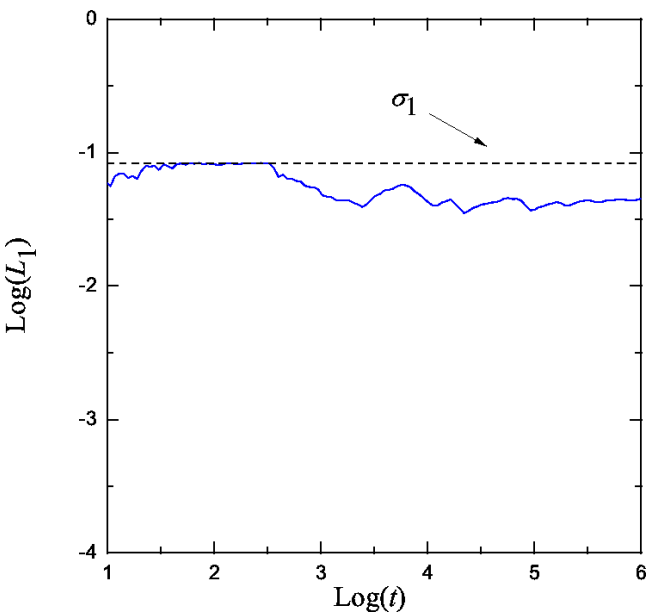

(e)

Fig. 1. (*Continued*)

4.2.2. *A 3dof Hamiltonian system*

Let us now investigate the behavior of the GALIs for a 3dof Hamiltonian system, where different types of unstable periodic orbits can appear. In particular, we consider a system of three harmonic oscillators with nonlinear coupling, described by the Hamiltonian

$$H_3 = \frac{1}{2}(p_x^2 + p_y^2 + p_z^2) + \frac{1}{2}(Ax^2 + By^2 + Cy^2) - \varepsilon x z^2 - \eta y z^2. \quad (25)$$

The harmonic frequencies of the oscillators are determined by parameters A, B, C, and the strengths of the nonlinear couplings by ε and η. This

system was introduced as a crude description of the inner parts of distorted three-dimensional elliptic galaxies. Detailed studies of its basic families of periodic orbits were performed in [Contopoulos & Barbanis, 1985; Contopoulos & Magnenat, 1985; Contopoulos, 1986a, 1986b]. Following these works, we fix $A = 0.9$, $B = 0.4$, $C = 0.225$ and $H_3 = 0.00765$ and vary ε and η in order to study periodic orbits of different stability types.

In Fig. 2(a) we plot the time evolution of GALIs for a stable (S_2) periodic orbit with initial condition $(x, y, z, p_x, p_y, p_z) \approx (-0.06686, 0.01230, 0, 0, 0, 0.10590)$ for $\varepsilon = 0.2$ and $\eta = 0.1$. The 3dof system has a six-dimensional phase space and so, five different GALI$_k$, with $2 \leq k \leq 6$, are defined. All GALIs decay to zero following the power law predictions given by Eq. (22) for $N = 3$.

Let us now study representative cases of all the different types of unstable periodic orbits that can appear in a general 3dof system. In particular, we consider an S_1U_1 periodic orbit with initial condition $(x, y, z, p_x, p_y, p_z) \approx (-0.0238841214, 0.0744533850, 0, 0, 0, 0.1121127613)$ for $\varepsilon = 0.848$, $\eta = 0.1$ [Fig. 2(b)], an U_2 periodic orbit with initial condition $(x, y, z, p_x, p_y, p_z) \approx (-0.0392937629, 0.0648373644, 0, -0.0564496390, 0.0021636015, 0.0950663122)$ for $\varepsilon = 0.35$, $\eta = 0.51$ [Fig. 2(c)], and a Δ_1 periodic orbit with initial condition $(x, y, z, p_x, p_y, p_z) \approx (-0.0456720106, 0.0658047594, 0, 0, 0, 0.1081228661)$ for $\varepsilon = 0.6$ and $\eta = 0.3$ [Figs. 2(d) and 2(e)].

Using Eq. (13) we estimated the LCEs to be $\sigma_1 \approx 0.046$, $\sigma_2 = 0$ and $\sigma_1 \approx 0.014$, $\sigma_2 \approx 0.0019$ for the S_1U_1 and the U_2 unstable periodic orbits, respectively. Using these values as good approximations of the actual LCEs, we see in Figs. 2(b) and 2(c) that the evolution of GALIs is well reproduced by Eq. (14).

An eigenvalue of the monodromy matrix of the Δ_1 unstable periodic orbit is numerically found to be $\lambda_1 \approx 1.410 + 0.164i$, while the remaining three of them (apart from the two unit ones) are $1/\lambda_1$, λ_1^* and $1/\lambda_1^*$. Then, from Eq. (13), we estimated the three largest LCEs of the periodic orbit to be $\sigma_1 = \sigma_2 \approx 0.023$, $\sigma_3 = 0$. The evolution of the GALIs for this orbit is shown in Fig. 2(d). Although the periodic orbit is unstable, GALI$_2$ does not decay to zero but remains constant until $t \approx 10^3$. This happens because, according to Eq. (14) GALI$_2 \propto e^{-(\sigma_1 - \sigma_2)t}$, but in this case $\sigma_1 = \sigma_2$. However,

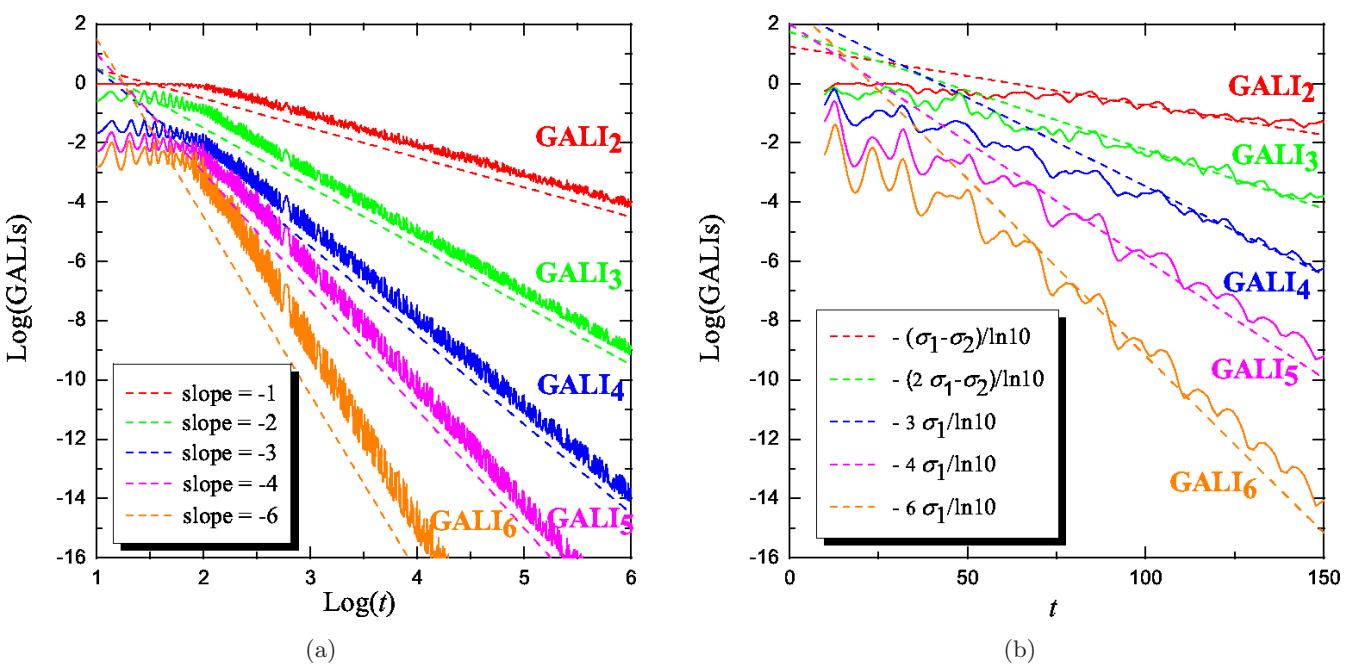

(a) (b)

Fig. 2. The time evolution of GALI$_k$, $2 \leq k \leq 6$ for (a) an S_2 stable, (b) an S_1U_1 unstable, (c) a U_2 unstable and (d) a Δ_1 unstable periodic orbit of the 3dof Hamiltonian system (25). Both axes of (a) and (d), and the vertical axis of (b) and (c) are logarithmic. Plotted lines correspond to appropriate power laws (22) in (a), and exponential laws (14) in (b) and (c). (e) The time evolution of quantities $L_1(t)$, $L_2(t)$ having respectively, as limit the two largest LCEs σ_1, σ_2 of the Δ_1 unstable periodic orbit. The theoretically estimated value $\sigma_1 = \sigma_2 = 0.023$ is denoted by a horizontal line.

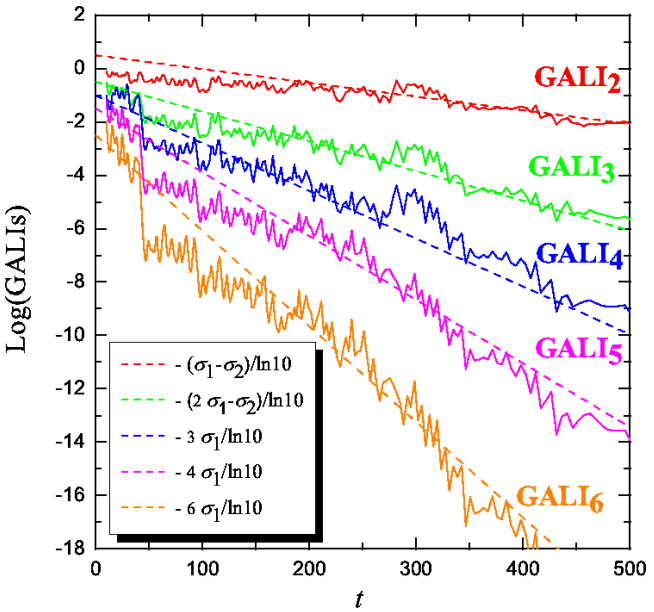

(c)

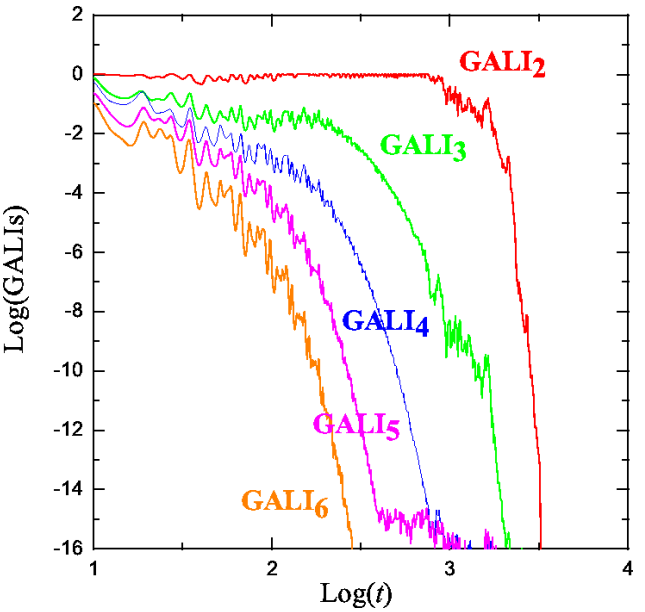

(d)

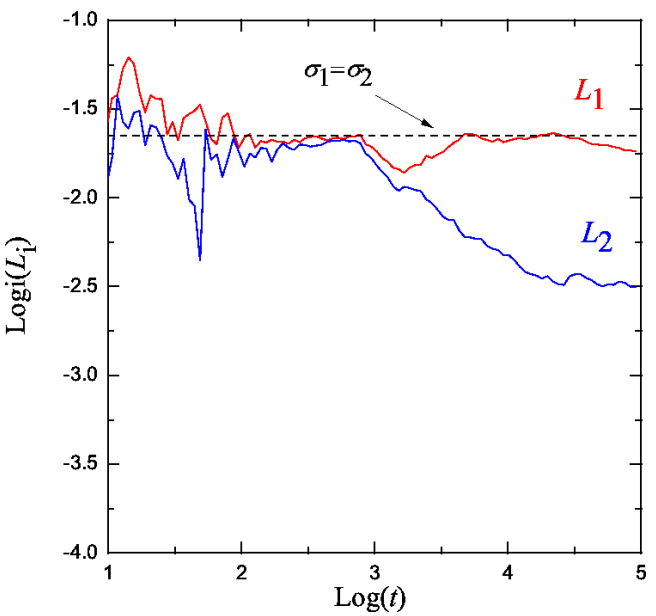

(e)

Fig. 2. (*Continued*)

due to unavoidable inaccuracies in the numerical integration, the computed orbit eventually diverges from the unstable periodic one and enters a chaotic domain characterized by different LCEs with $\sigma_1 \neq \sigma_2$. This divergence is also evident from the evolution of quantities $L_1(t)$, $L_2(t)$ in Fig. 2(e), whose limits at $t \to \infty$ are σ_1 and σ_2 respectively (see [Skokos, 2010] for more details on the computation of σ_1 and σ_2). In particular, we get $L_1(t) \approx L_2(t)$ for $t \lesssim 10^3$, while later on the two quantities attain different values. Consequently, for $t \gtrsim 10^3$ $GALI_2$ starts to decay exponentially to zero. On the other hand, all other GALIs in Fig. 2(d) show an exponential decay, even when $GALI_2$ remains constant, since the corresponding exponents in Eq. (14) do not vanish.

4.2.3. *A multidimensional Hamiltonian system*

Finally, we turn to a multidimensional Hamiltonian system representing a one-dimensional chain of five identical particles with nearest neighbor interactions given by the FPU-β Hamiltonian [Fermi *et al.*, 1955]

$$H_5 = \frac{1}{2}\sum_{j=1}^{5} p_j^2 + \sum_{j=0}^{5}\left(\frac{1}{2}(x_{j+1}-x_j)^2 + \frac{1}{4}\beta(x_{j+1}-x_j)^4\right), \tag{26}$$

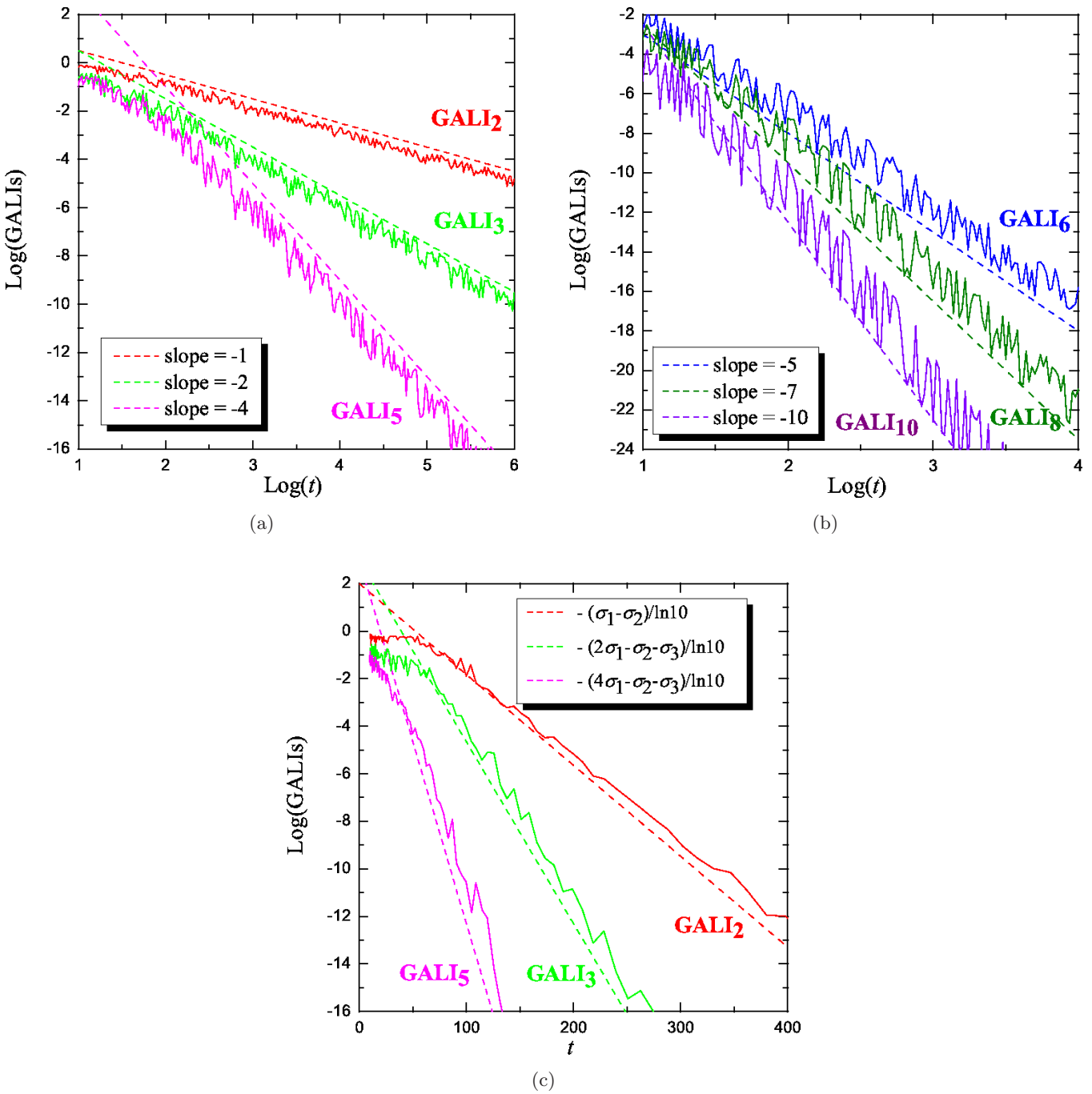

Fig. 3. The time evolution of (a) $GALI_2$, $GALI_3$, $GALI_5$ and (b) $GALI_6$, $GALI_8$, $GALI_{10}$ for a stable periodic orbit of the 5dof Hamiltonian system (26). (c) The time evolution of $GALI_2$, $GALI_3$, $GALI_5$ for an S_4U_1 unstable periodic orbit of the same model. Plotted lines correspond to appropriate power laws (22) in (a) and (b), and exponential laws (14) in (c).

where x_j is the displacement of the jth particle from its equilibrium position and p_j is the corresponding conjugate momentum. In our study, we set $\beta = 1.04$ and impose fixed boundary conditions to the system, so that we always have $x_0 = x_6 = 0$.

Let us consider two particular members of a family of periodic orbits studied in [Ooyama *et al.*, 1969; Antonopoulos *et al.*, 2006] which have initial conditions of the form $x_1(0) = -x_3(0) = x_5(0) = \hat{x}(0)$, $x_2(0) = x_4(0) = 0$, $p_j(0) = 0$, $1 \leq j \leq 5$. We compute the GALIs of an S_5 stable periodic orbit [Figs. 3(a) and 3(b)] with initial condition $\hat{x}(0) \approx 1.035$ for $H_5 = 5$ and an S_4U_1 unstable periodic orbit [Fig. 3(c)] with initial condition $\hat{x}(0) \approx 1.168$ for $H_5 = 7$. From Fig. 3 we see again that the behavior of the GALIs is well reproduced by Eq. (22) for $N = 5$ in the case of the stable orbit, and by Eq. (14) for $\sigma_1 = 0.088$, $\sigma_i = 0$, $2 \leq i \leq 5$, which are the values obtained by Eq. (13) for the unstable orbit.

4.3. *Numerical results — Symplectic maps*

According to the theoretical arguments of Sec. 4.1, the GALIs of unstable periodic orbits of maps should exhibit the same behavior as in the case of Hamiltonian flows, i.e. they should tend exponentially to zero following Eq. (14). On the other hand, we have argued that the GALIs of stable periodic orbits should remain constant, according to Eq. (23), having a different behavior with respect to Hamiltonian systems. To verify these predictions, we now proceed to study some periodic orbits in a 2D and a 4D symplectic map.

4.3.1. *2D Hénon map*

First we consider the 2D Hénon map [Hénon, 1969]

$$\begin{aligned} x' &= x\cos(2\pi\omega) + (y + x^2)\sin(2\pi\omega) \\ y' &= -x\sin(2\pi\omega) + (y + x^2)\cos(2\pi\omega), \end{aligned} \tag{27}$$

where ω is a real positive constant. The phase space of this map for $\omega = 0.201$ is plotted in Fig. 4(a). We consider two periodic orbits of period 5 (i.e. after five iterations of the map the orbit returns to its initial point): an S_1 stable orbit (blue stars in Fig. 4(a)) with initial condition $(x, y) \approx (0.14175, -0.10366)$, and an U_1 unstable one (red crosses in Fig. 4(a)) with initial condition $(x, y) \approx (0.0622148475, 0.1477550294)$. Figure 4(b) shows that the $GALI_2$ of the stable periodic orbit oscillates around a constant positive value, in accordance to Eq. (23). We have also verified that the $GALI_2$ of

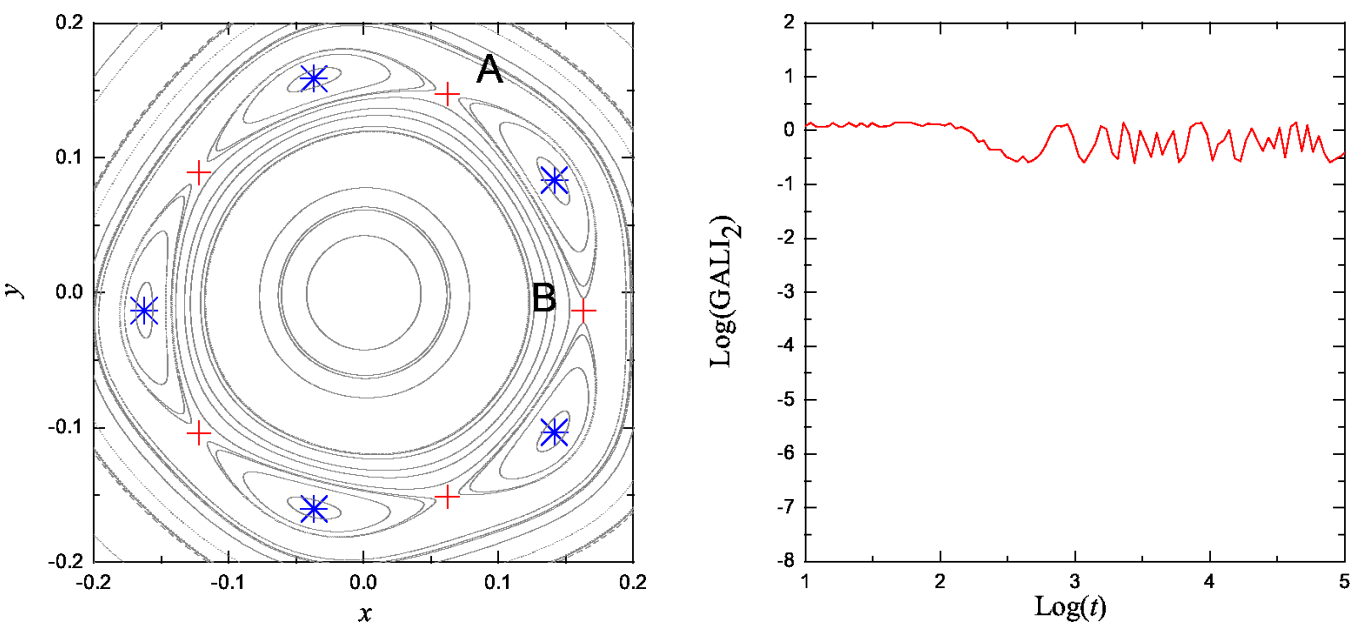

(a) (b)

Fig. 4. (a) The phase space of the 2D Hénon map (27) for $\omega = 0.201$. The points of two periodic orbits of period 5, a stable (blue stars) and an unstable one (red crosses), are also plotted. The time evolution of $GALI_2$ of the stable orbit is plotted in (b). Two particular points of the unstable periodic orbit discussed in Sec. 5 are marked by letters A and B.

the unstable periodic orbit decays exponentially to zero following Eq. (14) with $\sigma_1 = 0.0039$.

4.3.2. *4D standard map*

Let us now consider the 4D symplectic map [Kantz & Grassberger, 1988]

$$\begin{aligned} x_1' &= x_1 + x_2' \\ x_2' &= x_2 + \frac{K_1}{2\pi}\sin(2\pi x_1) \\ &\quad - \frac{\beta}{2\pi}\sin[2\pi(x_3 - x_1)] \\ &\quad \pmod 1, \qquad (28) \\ x_3' &= x_3 + x_4' \\ x_4' &= x_4 + \frac{K_2}{2\pi}\sin(2\pi x_3) \\ &\quad - \frac{\beta}{2\pi}\sin[2\pi(x_1 - x_3)] \end{aligned}$$

which consists of two coupled standard maps, with real parameters K_1, K_2 and β.

In Fig. 5 we plot the evolution of GALIs for an S_2 stable periodic orbit of period 7 with initial condition $(x_1, x_2, x_3, x_4) \approx (0.23666, 0, 0.23666, 0)$ for $K_1 = K_2 = 0.9$ and $\beta = 0.05$. Like in the case of the 2D map (27), $GALI_2$, $GALI_3$ and $GALI_4$ remain constant, oscillating around nonzero values, in accordance with Eq. (23).

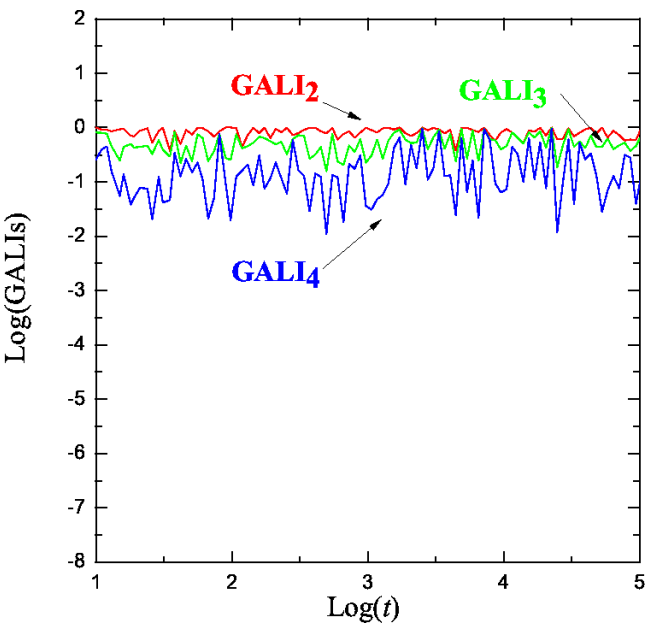

Fig. 5. The time evolution of $GALI_2$ (red curve), $GALI_3$ (green curve) and $GALI_4$ (blue curve) for a stable periodic orbit of period 7 of the 4D map (28).

5. Dynamics in the Neighborhood of Periodic Orbits

We now turn our attention to the dynamics in the *vicinity* of periodic orbits, studying initially the neighborhood of stable periodic orbits in Hamiltonian systems. As a first example, we consider the 2dof Hénon–Heiles system (24), and in particular, the stable periodic orbit of period 5 studied in Sec. 4.2.1. In Fig. 1(b), we have seen that $GALI_2 \propto t^{-1}$, $GALI_3 \propto t^{-2}$ and $GALI_4 \propto t^{-4}$ in accordance with Eq. (22). We expect that small perturbations of this trajectory will lead to regular motion on two-dimensional tori surrounding the periodic orbit. For this kind of motion, Eq. (7) predicts $GALI_2 \propto$ const, $GALI_3 \propto t^{-2}$ and $GALI_4 \propto t^{-4}$. Thus, only for $GALI_2$ a different evolution between the periodic orbit and its neighborhood is expected. This is actually true, as we see in Fig. 6(a) where the time evolution of $GALI_k$, $k = 2, 3, 4$ is plotted for the stable periodic orbit (red curves) and two nearby orbits whose initial conditions result from $\Delta y = 0.00793$ (green curves) and $\Delta y = 0.02793$ (blue curves) perturbations. The $GALI_2$ of neighboring orbits initially follows a $GALI_2 \propto t^{-1}$ evolution, similar to the periodic orbit, but later on stabilizes to a nonzero value as Eq. (7) predicts. From Fig. 6(a), we see that the closer the orbit is to the periodic trajectory the longer the initial phase of $GALI_2 \propto t^{-1}$ lasts, and the smaller is the final nonzero value to which the index tends.

Let us now perform a more global study of the dynamics of the Hénon–Heiles system. First, we consider orbits whose initial conditions lie on the $p_y = 0$ line of the PSS of Fig. 1(a). In particular, we use 7000 equally spaced initial conditions on this line and compute their $GALI_2$ values, using for each of them the same set of initial (random and orthonormal) deviation vectors. In Fig. 6(b), we plot the $GALI_2$ values at $t = 10^5$ as a function of y. The regions where $GALI_2$ has large values ($\gtrsim 10^{-1}$) correspond to regular motion on two-dimensional tori. Regions where $GALI_2$ has very small values ($\lesssim 10^{-12}$) correspond to chaotic or unstable periodic orbits, while domains with intermediate values ($10^{-4} \gtrsim GALI_2 \gtrsim 10^{-12}$), correspond to sticky, chaotic orbits. We also distinguish narrow regions where $GALI_2$ decreases abruptly to values $10^{-1} \gtrsim GALI_2 \gtrsim 10^{-4}$. These correspond to

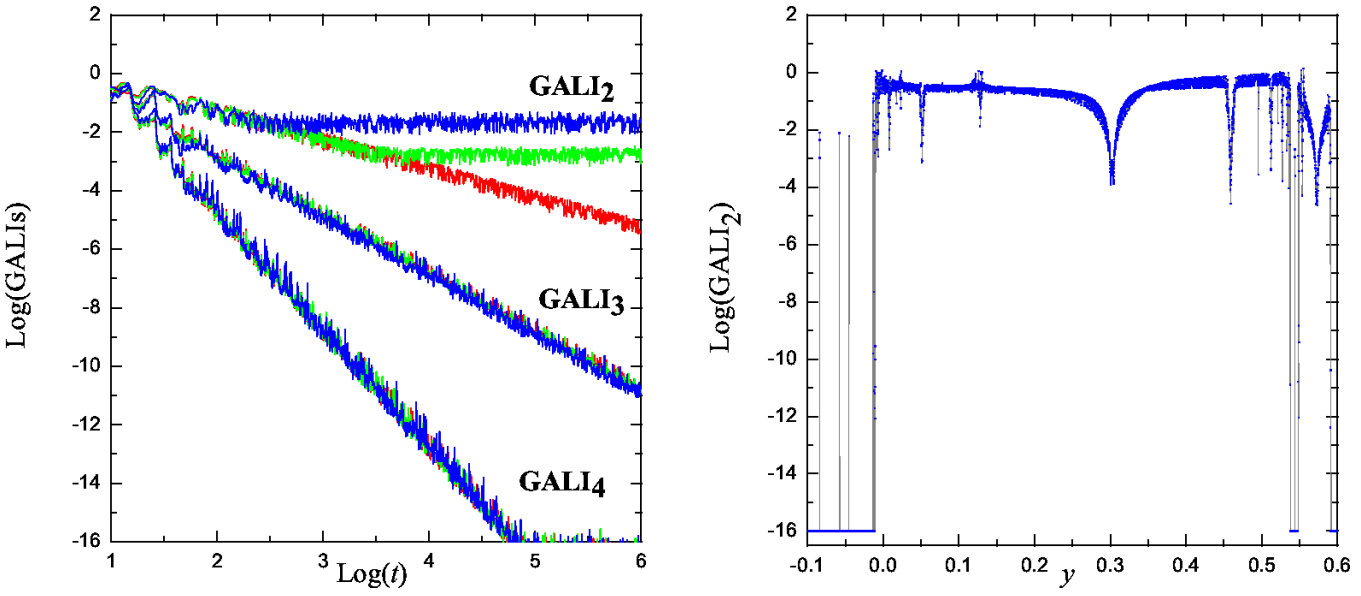

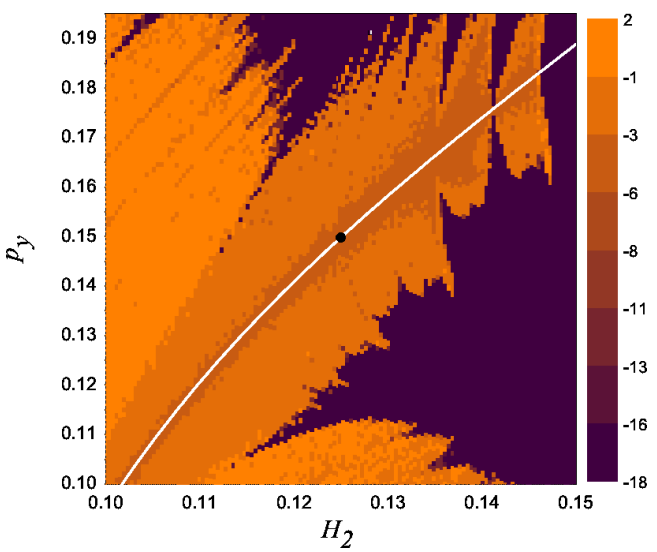

Fig. 6. (a) The time evolution of $GALI_2$, $GALI_3$ and $GALI_4$ for three orbits of the Hénon–Heiles system (24): The stable periodic orbit of period 5 studied in Sec. 4.2.1 (red curves) and two nearby orbits whose initial conditions result from $\Delta y = 0.00793$ (green curves) and $\Delta y = 0.02793$ (blue curves) perturbations of the periodic orbit. Note that curves of $GALI_3$ and $GALI_4$ overlap each other. (b) The $GALI_2$ values at $t = 10^5$ for orbits with initial conditions on the $p_y = 0$ line of the PSS of Fig. 1(a), as a function of the y coordinate of the initial condition. (c) Regions of different $GALI_2$ values on the (H_2, p_y) plane of the Hénon–Heiles system (24). Each point corresponds to an orbit in the neighborhood of a family of periodic orbits (white curve) and is colored according to the $\log(GALI_2)$ value computed at $t = 10^4$. The black filled circle denotes the stable periodic orbit of Fig. 1(b).

domains of regular motion around the main stable periodic orbits of the system, as e.g. in the vicinity of $y \approx 0.3$ which corresponds to the stable periodic orbit in the center of the main island of stability in the PSS of Fig. 1(a). This behavior appears because $GALI_2$ at stable periodic orbits decays following a t^{-1} power law and reaches values smaller than the ones obtained for the neighboring regular orbits, where $GALI_2$ tends to constant nonzero values, as we have seen in Fig. 6(a).

This information can be directly used to identify the location of stable periodic orbits. In Fig. 6(c) we show a color plot of the parametric space (H_2, p_y) of the Hénon–Heiles system (24). Each point corresponds to an initial condition and is colored according to its $\log(\mathrm{GALI}_2)$ value computed at $t = 10^4$. Chaotic orbits are characterized by very small GALI_2 values and are located in the purple colored domains. The deep orange colored "strip" corresponds to the vicinity of a family of stable periodic orbits (this family is denoted by a white curve) for which GALI_2 attains smaller (but not too small) values with respect to the surrounding light orange colored region, where regular motion on two-dimensional tori takes place. We note that, as H_2 increases, the periodic orbit changes its stability

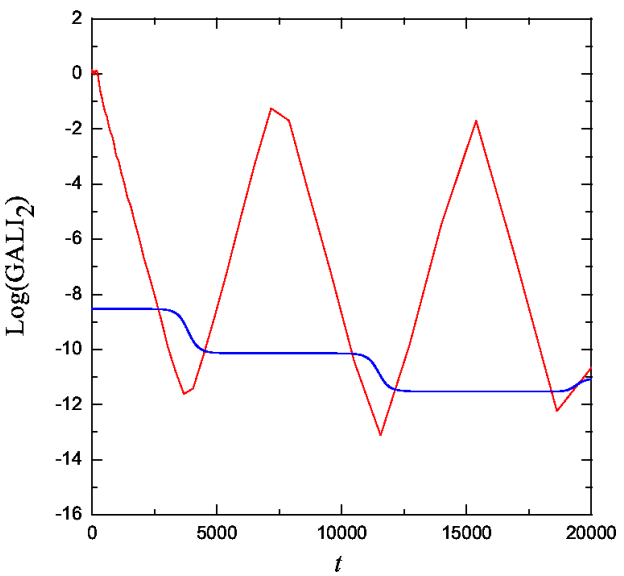

(a)

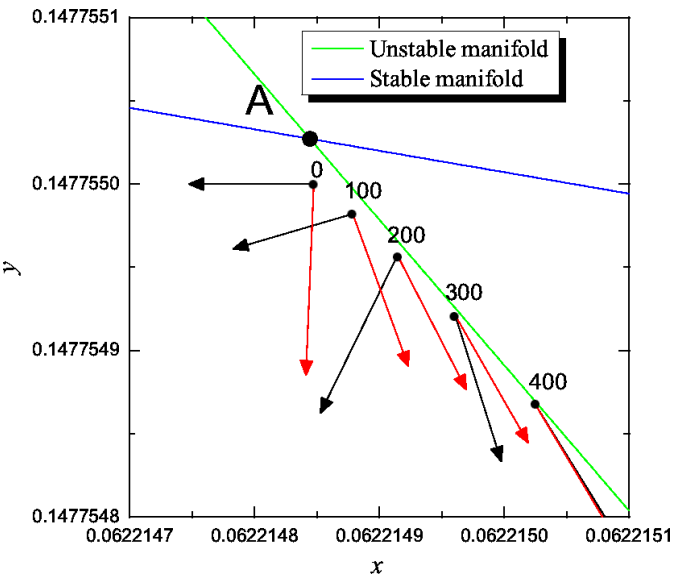

(b)

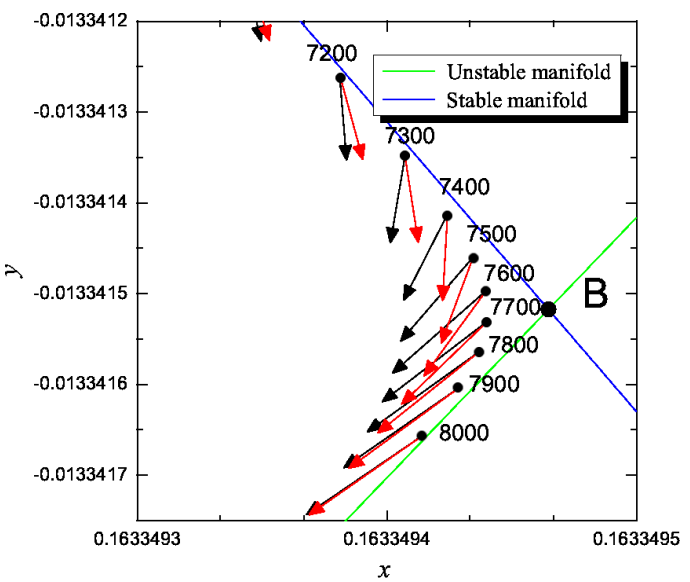

(c)

Fig. 7. (a) The time evolution of GALI_2 of a chaotic orbit of the 2D map (27), with initial condition close to the unstable periodic orbit discussed in Sec. 4.3.1. The blue curve shows the y coordinate of the orbit in arbitrary units. Consequents of this orbit and its two unit deviation vectors in the neighborhood of points A and B of the unstable periodic orbit of Fig. 4(a), are respectively plotted in (b) and (c). In (b) and (c) the stable and unstable manifolds of points A and B are respectively plotted, while the points of the chaotic orbit are labeled according to their iteration number.

and becomes unstable for $H_2 \gtrsim 0.146$. The point $H_2 = 0.125$, $p_y = 0.14979$, denoted by a black filled circle in Fig. 6(c), corresponds to the stable periodic orbit of Fig. 1(b).

The GALIs of chaotic orbits in the vicinity of unstable periodic orbits can exhibit a remarkable oscillatory behavior. Such an example is shown in Fig. 7 for a chaotic orbit of the 2D map (27) with initial condition $(x, y) = (0.06221484498946357, 0.14775502681732178)$ (point denoted by "0" in Fig. 7(b)), which is located very close to the unstable periodic orbit of period 5 discussed in Sec. 4.3.1 (point A in Figs. 4(a) and 7(b)). In Fig. 7(a) we see that the $GALI_2$ of this orbit decreases exponentially, reaching very small values ($GALI_2 \approx 10^{-12}$), since the two initially orthonormal deviation vectors tend to align [Fig. 7(b)] due to the chaotic nature of the orbit.

The evolution of these vectors is strongly influenced by the stable and unstable manifolds of the nearby unstable periodic orbit. In particular, as the chaotic orbit moves away from point A along a direction parallel to the unstable manifold (green curve in Fig. 7(b)), both deviation vectors are stretched in this direction, and shrunk in the direction of the stable manifold (blue curve in Fig. 7(b)). So, after a few hundreds of iterations, while the orbit remains in the proximity of point A (note the tiny intervals in both axes of Fig. 7(b)), the evolved unit deviation vectors become almost identical, and consequently $GALI_2$ decreases significantly.

Nevertheless, the angle between the two vectors does not vanish, and starts to grow again when the orbit approaches point B of Fig. 7(c), which is the next consequence of the unstable periodic orbit (see also Fig. 4(a)). The chaotic orbit approaches point B moving parallel to the stable manifold of point B (blue curve in Fig. 7(c)). Now the deviation vectors start to shrink along this manifold, while they expand along the direction of the unstable manifold of point B (green curve in Fig. 7(c)). This leads to a significant increase of the angle between the two unit vectors, as we see in Fig. 7(c), and consequently to an increase of the $GALI_2$ values [Fig. 7(a)].

This oscillatory behavior is repeated as the chaotic orbit visits all consequents of the unstable periodic orbit, and is clearly seen in Fig. 7(a) where the y coordinate of the chaotic orbit is plotted in arbitrary units (blue curve) together with the $GALI_2$ values. The horizontal segments of this curve correspond to the time intervals that the orbit spends close to the fixed points of the unstable periodic orbit. During the first part of these intervals the chaotic orbit approaches a fixed point, the two deviation vectors become different and $GALI_2$ increases, while afterwards, the chaotic orbit moves away from the fixed point, whence the two deviation vectors tend to align, and $GALI_2$ decreases.

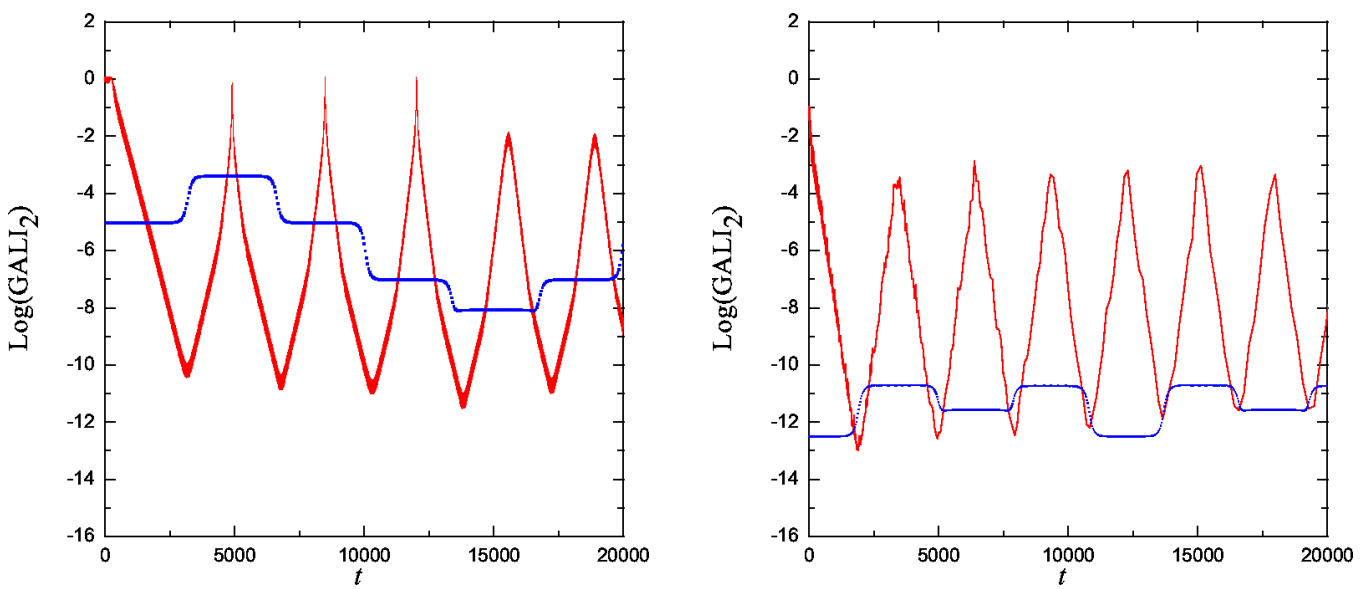

(a) (b)

Fig. 8. Plots similar to Fig. 7(a) for orbits of (a) the 2dof Hénon–Heiles system (24), and (b) the 3dof Hamiltonian system (25). Blue curves show in arbitrary units the y coordinate of the studied orbits on (a) the PSS $x = 0$, $p_x \geq 0$ of system (24), and (b) the PSS $z = 0$, $p_z \geq 0$ of system (25).

$GALI_2$ reaches its lowest values during the short transition intervals between the neighborhoods of two successive points of the unstable periodic orbit, which correspond to the short connecting segments between the plateaus of the blue curve in Fig. 7(a). These oscillations of $GALI_2$ can last for quite long time intervals, but eventually the chaotic orbit will escape from the strong influence of the homoclinic tangle of the unstable periodic orbit and $GALI_2$ will rapidly tend to zero. It is worth mentioning that abrupt changes in the values of SALI (which practically is $GALI_2$) by many orders of magnitude were also reported in [Voyatzis, 2008] for chaotic orbits of planetary systems.

Up to now, we have described in detail these oscillations of $GALI_2$ in the case of the 2D map (27) because they can be easily explained, while the deviation vectors themselves can be visualized in the two-dimensional phase space of the map. Interestingly, this remarkable behavior occurs in higher dimensional systems as well. In Fig. 8 we show two such examples. In particular, we consider a chaotic orbit of the 2dof Hamiltonian system (24), whose initial condition is located close to an unstable periodic orbit of period 7 with initial condition $(x, y, p_x, p_y) \approx (0, 0.1282112414, 0.4847338571, 0)$ [Fig. 8(a)], and an orbit of the 3dof system (25) whose initial condition is near the S_1U_1 periodic orbit presented in Sec. 4.2.2 [Fig. 8(b)]. In both panels of Fig. 8 we observe an oscillatory behavior of $GALI_2$, similar to the one shown in Fig. 7(a). We also point out that in both cases all other GALIs show similar oscillatory behaviors.

6. Connection Between the Dynamics of Flows and Maps

In Sec. 3 we discussed the dynamical equivalence between Ndof Hamiltonian systems and $2(N-1)$D maps, as the latter can be interpreted as appropriate PSSs of the former. We have also seen that GALIs behave differently for flows and maps. In particular, as was shown in Sec. 4, they remain constant for stable periodic orbits of maps [see Eq. (23)] and decrease to zero for flows, according to Eq. (22).

The fact that maps can be considered as PSS of flows, however, is the key to understanding this difference. So, computing the restriction of the GALIs on the PSS of a Hamiltonian system, or more generally on spaces perpendicular to the flow, should lead to behaviors of the indices similar to the ones obtained for maps. Actually this approach has already been successfully applied to other chaos indicators related to the evolution of deviation vectors [Fouchard *et al.*, 2002; Barrio, 2005], by only

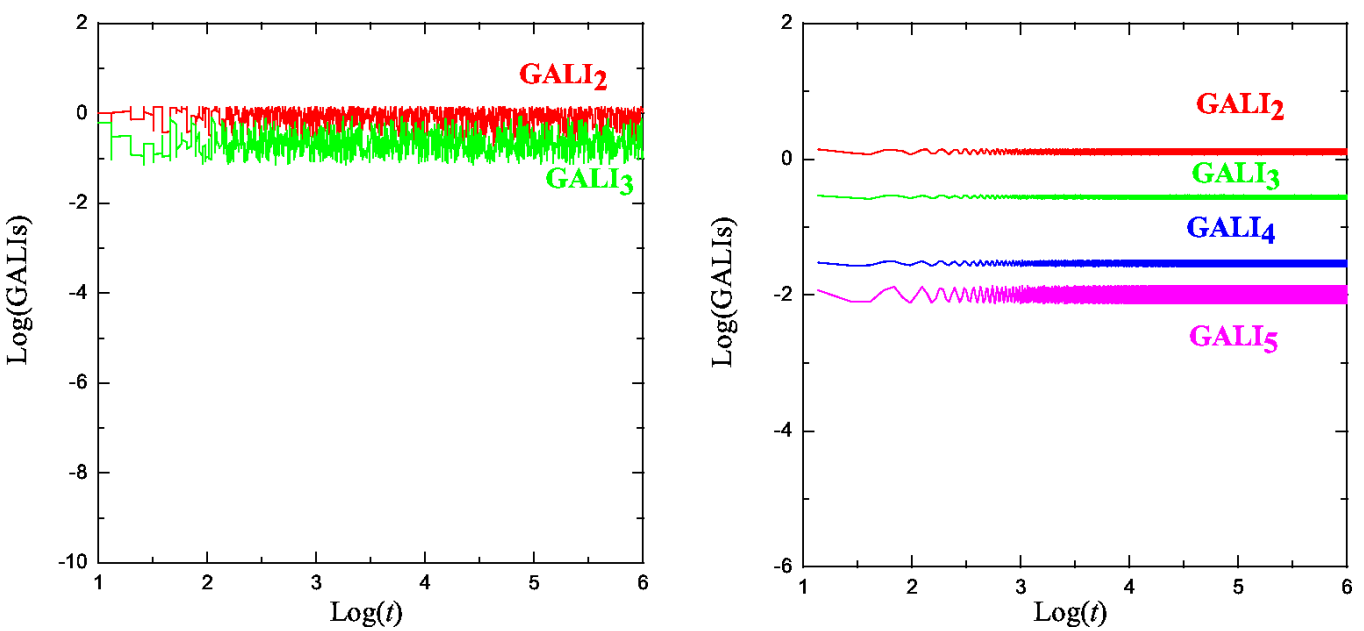

(a) (b)

Fig. 9. The time evolution of (a) $GALI_k$, $k = 2, 3$ for the stable periodic orbit of the 2dof system (24) presented in Fig. 1(b), and (b) $GALI_k$, $k = 2, 3, 4, 5$ for the stable periodic orbit of the 3dof system (25) presented in Fig. 2(a), when the orthogonal to the flow components of the deviation vectors are used.

considering the components of these vectors which are orthogonal to the flow.

Using deviation vectors orthogonal to the flow, we indeed obtain the same GALI behavior for stable periodic orbits of flows and maps. Now, for stable periodic orbits of flows the GALIs of these vectors remain constant, as we see from Figs. 9(a) and 9(b) where these GALIs are plotted for the stable periodic orbits of Figs. 1(b) and 2(a), respectively. These behaviors differ, however, from the ones shown in Figs. 1(b) and 2(a) where the GALIs of the usual deviation vectors were computed. We note that when vectors orthogonal to the flow are used, $GALI_{2N}$ of an Ndof Hamiltonian system is by definition equal to zero, because the $2N$ projected vectors are linearly dependent on a $(2N-1)$-dimensional space. For this reason, $GALI_4$ and $GALI_6$ are not displayed in Figs. 9(a) and 9(b) respectively.

7. Summary

In this paper, we have explored in more detail the properties of the GALI method by using it to study the local dynamics of periodic solutions of conservative dynamical systems. To this end, we have: (a) theoretically predicted and numerically verified the behavior of the method for periodic orbits, (b) summarized the expected behaviors of the indices and (c) clarified the connection between the behavior of GALIs for dynamical systems of continuous (Hamiltonian flows) and discrete (symplectic maps) time.

More specifically, we showed that for stable periodic orbits, GALIs tend to zero following particular power laws for Hamiltonian flows [Eq. (22)], while they fluctuate around nonzero values for symplectic maps [Eq. (23)]. In addition, the GALIs of unstable periodic orbits tend exponentially to zero, both for flows and maps [Eq. (8)].

Finally, we examined the usefulness of the indices in helping us better understand the dynamics in the vicinity of periodic solutions of such systems. We explained how, the fact that GALIs attain larger values *near* stable periodic orbits than *on* the periodic orbits themselves, can be used to identify the location of these orbits. We also observed a remarkable oscillatory behavior of the GALIs associated with the dynamics close to unstable periodic orbits and explained it in terms of the stable and unstable manifolds of the periodic orbit, showing how the influence of these manifolds can lead to large variations of the GALI values by many orders of magnitude.

Acknowledgments

The authors thank T. Bountis for many valuable suggestions and comments on the content of the manuscript. Ch. Skokos would like to thank A. Celletti and A. Ponno for useful discussions and T. Manos, the Max Planck Institute for the Physics of Complex Systems in Dresden, Germany, for its hospitality during his visit in May–June 2009, where a significant part of this work was performed. This work was partly supported by the European research project "Complex Matter", funded by the GSRT of the Ministry Education of Greece under the ERA-Network Complexity Program. Ch. Antonopoulos was also supported by the PAI 2007–2011 "NOSY-Nonlinear systems, stochastic processes and statistical mechanics" (FD9024CU1341) contract of ULB.

References

Antonopoulos, Ch. & Bountis, T. [2006] "Detecting order and chaos by the linear dependence index," *ROMAI J.* **2**, 1–13.

Antonopoulos, C., Bountis, T. & Skokos, C. [2006] "Chaotic dynamics of N-degree of freedom Hamiltonian systems," *Int. J. Bifurcation and Chaos* **16**, 1777–1793.

Barrio, R. [2005] "Sensitivity tools vs. Poincaré sections," *Chaos Solit. Fract.* **25**, 711–726.

Benettin, G. & Galgani, L. [1979] "Lyapunov characteristic exponents and stochasticity," in *Intrinsic Stochasticity in Plasmas*, eds. Laval, G. & Grésillon, D. (Edit. Phys. Orsay), pp. 93–114.

Benettin, G., Froeschlé, C. & Scheidecker, J. P. [1979] "Kolmogorov entropy of a dynamical system with an increasing number of degrees of freedom," *Phys. Rev. A* **19**, 2454–2460.

Bountis, T. & Skokos, Ch. [2006] "Application of the SALI chaos detection method to accelerator mappings," *Nucl. Instr. Meth. Phys. Res. — Sect. A* **561**, 173–179.

Bountis, T., Manos, T. & Christodoulidi, H. [2009] "Application of the GALI method to localization dynamics in nonlinear systems," *J. Comp. Appl. Math.* **227**, 17–26.

Broucke, R. A. [1969] "Periodic orbits in restricted three body problem," NASA Tech. Rep. 32-1360.

Capuzzo-Dolcetta, R., Leccese, L., Merritt, D. & Vicari, A. [2007] "Self-consistent models of cuspy triaxial galaxies with dark matter halos," *Astrophys. J.* **666**, 165–180.

Christodoulidi, H. & Bountis, T. [2006] "Low-dimensional quasiperiodic motion in Hamiltonian systems," *ROMAI J.* **2**, 37–44.

Contopoulos, G. & Barbanis, B. [1985] "Resonant systems with three degrees of freedom," *Astron. Astrophys.* **153**, 44–54.

Contopoulos, G. & Magnenat, P. [1985] "Simple three-dimensional periodic orbits in a galactic-type potential," *Celest. Mech.* **37**, 387–414.

Contopoulos, G. [1986a] "Qualitative changes in 3-dimensional dynamical systems," *Astron. Astrophys.* **161**, 244–256.

Contopoulos, G. [1986b] "Bifurcations in systems of three degrees of freedom," *Celest. Mech.* **38**, 1–22.

Cvitanović, P., Artuso, R., Mainieri, R., Tanner, G. & Vattay, G. [2009] *Chaos*: *Classical and Quantum* (Niels Bohr Institute, Copenhagen).

Dullin, H. R. & Meiss, J. D. [1998] "Stability of minimal periodic orbits," *Phys. Lett. A* **247**, 227–234.

Fermi, E., Pasta, J. & Ulam, S. [1955] "Studies of nonlinear problems," Los Alamos document LA-1940; [1974] "Nonlinear wave motion" *Am. Math. Soc. Providence*, **15**, Lectures in Appl. Math., ed. Newell, A. C.

Fouchard, M., Lega, E., Froeschlé, Ch. & Froeschlé, C. [2002] "On the relationship between the fast Lyapunov indicator and periodic orbits for continuous flows," *Celest. Mech. Dyn. Astron.* **83**, 205–222.

Gerlach, E., Eggl, S. & Skokos, Ch. [2012] "Efficient integration of the variational equations of multi-dimensional Hamiltonian systems: Application to the Fermi–Pasta–Ulam lattice," *Int. J. Bifurcation and Chaos* **22**.

Hadjidemetriou, J. [1975] "The stability of periodic orbits in the three-body problem," *Celest. Mech.* **12**, 255–276.

Hadjidemetriou, J. [2006] "Periodic orbits in gravitational systems," *Chaotic Worlds*: *From Order to Disorder in Gravitational N-Body Dynamical Systems, Proc. Advanced Study Institute*, eds. Steves, B. A., Maciejewski, A. J. & Hendry, M., pp. 43–79.

Hénon, M. & Heiles, C. [1964] "The applicability of the third integral of motion: Some numerical experiments," *Astron. J.* **69**, 73–79.

Hénon, M. [1969] "Numerical study of quadratic area-preserving mappings," *Quart. Appl. Math.* **27**, 291–312.

Howard, J. E. & MacKay, R. S. [1987] "Linear stability of symplectic maps," *J. Math. Phys.* **28**, 1036–1051.

Howard, J. E. & Dullin, H. R. [1998] "Linear stability of natural symplectic maps," *Phys. Lett. A* **246**, 273–283.

Kantz, H. & Grassberger, P. [1988] "Internal Arnold diffusion and chaos thresholds in coupled symplectic maps," *J. Phys. A*: *Math. Gen* **21**, L127–133.

Lega, E. & Froeschlé, C. [2001] "On the relationship between fast Lyapunov indicator and periodic orbits for symplectic mappings," *Celest. Mech. Dyn. Astron.* **81**, 129–147.

Lichtenberg, A. J. & Lieberman, M. A. [1992] *Regular and Chaotic Dynamics*, 2nd edition (Springer Verlag, Berlin).

Macek, M., Stránský, P., Cejnar, P., Heinze, S., Jolie, J. & Dobeš, J. [2007] "Classical and quantum properties of the semiregular arc inside the Casten triangle," *Phys. Rev. C* **75**, 064318.

Macek, M., Dobeš, J., Stránský, P. & Cejnar, P. [2010] "Regularity-induced separation of intrinsic and collective dynamics," *Phys. Rev. Lett.* **105**, 072503.

Manos, T., Skokos, Ch. & Bountis, T. [2008a] "Application of the generalized alignment index (GALI) method to the dynamics of multi-dimensional symplectic maps," *Chaos*, *Complexity and Transport*: *Theory and Applications. Proc. CCT07*, eds. Chandre, C., Leoncini, X. & Zaslavsky, G., pp. 356–364.

Manos, T., Skokos, Ch., Athanassoula, E. & Bountis, T. [2008b] "Studying the global dynamics of conservative dynamical systems using the SALI chaos detection method," *Nonlin. Phenom. Compl. Syst.* **11**, 171–176.

Manos, T., Skokos, Ch. & Bountis, T. [2009] "Global dynamics of coupled standard maps," *Chaos in Astronomy*, eds. Contopoulos, G. & Patsis, P. A., Astrophysics and Space Science Proc., pp. 367–371.

Manos, T. & Athanassoula, E. [2011] "Regular and chaotic orbits in barred galaxies — I. Applying the SALI/GALI method to explore their distribution in several models," *Mon. Not. R. Astron. Soc.* **415**, 629–642.

Manos, T. & Ruffo, S. [2011] "Scaling with system size of the Lyapunov exponents for the Hamiltonian mean field model," *Transp. Th. Statist. Phys.* **40**, 360–381.

Ooyama, N., Hirooka, H. & Saito, N. [1969] "Computer studies on the approach to thermal equilibrium in coupled anharmonic oscillators. II. One dimensional case," *J. Phys. Soc. Japan* **27**, 815–824.

Panagopoulos, P., Bountis, T. & Skokos, Ch. [2004] "Existence and stability of localized oscillations in 1-dimensional lattices with soft spring and hard spring potentials," *J. Vibr. Acoust.* **126**, 520–527.

Skokos, Ch. [2001a] "On the stability of periodic orbits of high dimensional autonomous Hamiltonian systems," *Physica D* **159**, 155–179.

Skokos, Ch. [2001b] "Alignment indices: A new, simple method for determining the ordered or chaotic nature of orbits," *J. Phys. A* **34**, 10029–10043.

Skokos, Ch., Antonopoulos, C., Bountis, T. & Vrahatis, M. N. [2003] "How does the Smaller Alignment Index (SALI) distinguish order from chaos?" *Prog. Theor. Phys. Supp.* **150**, 439–443.

Skokos, Ch., Antonopoulos, Ch., Bountis, T. & Vrahatis, M. N. [2004] "Detecting order and chaos in Hamiltonian systems by the SALI method," *J. Phys. A* **37**, 6269–6284.

Skokos, Ch., Bountis, T. & Antonopoulos, Ch. [2007] "Geometrical properties of local dynamics in Hamiltonian systems: The Generalized Alignment Index (GALI) method," *Physica D* **231**, 30–54.

Skokos, Ch., Bountis, T. & Antonopoulos, Ch. [2008] "Detecting chaos, determining the dimensions of tori and predicting slow diffusion in Fermi–Pasta–Ulam lattices by the Generalized Alignment Index method," *Eur. Phys. J. Sp. Top.* **165**, 5–14.

Skokos, Ch. [2010] "The Lyapunov characteristic exponents and their computation," *Lecture Notes in Physics* **790**, 63–135.

Skokos, Ch. & Gerlach, E. [2010] "Numerical integration of variational equations," *Phys. Rev. E* **82**, 036704.

Stránský, P., Hruška, P. & Cejnar, P. [2009] "Quantum chaos in the nuclear collective model: Classical-quantum correspondence," *Phys. Rev. E* **79**, 046202.

Széll, A., Érdi, B., Sándor, Z. & Steves, B. [2004] "Chaotic and stable behaviour in the Caledonian symmetric four-body problem," *Mon. Not. R. Astron. Soc.* **347**, 380–388.

Voyatzis, G [2008] "Chaos, order, and periodic orbits in 3:1 resonant planetary dynamics," *Astrophys. J.* **675**, 802–816.